AIMS Mathematics, 8(2): 3163–3184.
DOI:10.3934/math.2023162
Received: 27 July 2022
Revised: 25 October 2022
Accepted: 30 October 2022
Published: 16 November 2022

http://www.aimspress.com/journal/Math

Research article

Rational solutions of an extended (2+1)-dimensional Camassa-Holm-Kadomtsev-Petviashvili equation in liquid drop

Zhe Ji[1], Yifan Nie[2], Lingfei Li[1,*], Yingying Xie[3] and Mancang Wang[1]

[1] School of Economics and Management, Northwest University, Xi'an 710127, Shaanxi, China
[2] School of Business Administration, Xi'an Eurasia University, Xi'an 710065, Shaanxi, China
[3] School of Mathematics and Statistics, Xi'an Jiaotong University, Xi'an 710049, Shaanxi, China

* **Correspondence:** Email: infei2006@163.com.

Abstract: This paper investigates rational solutions of an extended Camassa-Holm-Kadomtsev-Petviashvili equation, which simulates dispersion's role in the development of patterns in a liquid drop, and describes left and right traveling waves like the Boussinesq equation. Through its bilinear form and symbolic computation, we derive some multiple order rational and generalized rational solutions and analyze their dynamic features, such as the connection between rational solution and bilinear equation, scatter behavior, moving path, and exact location of the soliton. The obtained solutions demonstrate two wave forms: multi-lump and multi-wave that consist of three, six and eight lump waves or two, three and four line waves. Moreover, different from the multi-wave solitons, stationary multiple dark waves are presented.

Keywords: CH-KP equation; rogue wave; rational solution; symbolic computation
Mathematics Subject Classification: 35A08, 35C05, 35C07, 35C08, 35C11

1. Introduction

"A rogue wave" is a single wave that comes out in the ocean "from nowhere" with a much higher amplitude than the average crests around it [1]. It was thought to be mystical until someone had a similar experience [2]. Those who are involved in such a disaster surely will focus on saving lives rather than recording evidence [3]. For such reason, there does not exist a clear understanding of this occurrence until now [4]. The superposition principle based on linear theory is inadequate to explain large amplitude, but nonlinear theory would be more helpful [5]. There are two main characteristics of rogue waves: "appear from nowhere" and "disappear without a trace." The first characteristic lies in modulation instability as the solution encounters abnormal initial input that will increase exponentially [6]. On the other hand, Bespalov-Talanov instability does not last long and will return the solution

to its initial state [7]. As a result, in a conservative nonlinear system, each wave that "appears from nowhere" must "disappear without a trace" [8]. In contrast to soliton solution, lump solution is a kind of rational function solution that is localized in each direction [9]. A general rational solution was presented for an integrable system such as the KdV equation, the Boussinesq equation, the Toda lattice equation via the Wronskian and Casoratian determinant method.

Lately, Tian derived lump solution, multi-kink soliton and discussed the interaction between tripe and lump soliton from a (3+1)-dimensional Kadomtsev-Petviashvili equation with the help of Hirota's bilinear method and the Bäcklund transformation [10]. Moreover, the mechanism and transition of the solution have been investigated for the (2+1)-dimensional Sawada-Kotera equation using phase shift analysis and characteristic line [11]. It is worth noting that the $\bar{\partial}$-dressing method is proposed by Tian to study the three-component couple Hirota(tcCH) equation [12]. The coupled Maxwell-Bloch equations and the AKNS type integrable shallow water wave equation are studied by Darboux transformation [13–15]. Other work that involves Darboux transformation and symmetry condition can be seen in [16]. Recently, the consistent Riccati expansion method and the consistent tanh expansion method are employed to investigate KdV equation [17, 18]. Bäcklund-transformation and symbolic computation are also effective in dealing with nonlinear models [19–24].

In 1993, Camassa and Holm derived a completely integrable dispersive shallow water wave equation via Hamiltonian methods, i.e.,

$$u_t + 2ku_x - u_{xxt} + auu_x = 2u_xu_{xx} + uu_{xxx}, \tag{1.1}$$

where $u = u(x, t)$ is the height of the water's free surface over a flat bottom, related to the spatial coordinate x and time t; k is a constant that has to do with the shallow water wave speed; the subscripts stand for the partial derivatives [25]. As a small amplitude expansion of incompressible Euler's equations for unidirectional wave motion at the free surface under the influence of gravity, the higher order terms (the right-hand side) are usually neglected in the small amplitude, shallow water limit [26]. Leaving those terms brings about the Benjamin-Bona-Mahony equation or the Korteweg-de Vries equation in the same order [27]. Therefore, the Camassa-Holm(CH) equation can be treated as an extension of the Benjamin-Bona-Mahony(BBM) equation [28, 29]. This extension renders solitons whose limiting form($k \to 0$) is peak as their first derivative is discontinued(compared with the smooth isolated waves) [30]. Such "peakons" dominate the solutions of the initial value problems under the condition of $k = 0$, i.e.,

$$u(x, t) = ce^{-|x-ct|},$$

where c is the wave speed, which means u has slope discontinuities [31]. If a derivative discontinuity occurs, we can limit a verticality at each inflection point to break a smooth initial condition into a series of peakons. Moreover, multisolitons can be obtained by superimposing the single solitons and solving as a completely integrable finite dimensional bi-Hamiltonian system, i.e., it can be written in two different kinds of Hamiltonian forms [32]. It is this property modifies the CH equation as a compatibility condition for a linear isospectral problem, such that the inverse scattering transformation can solve the initial value problem. Boyd pointed out why CH equation is important: it is a shallow water model like the KdV equation; two is it gives the peaked periodic waves with discontinuous first derivatives [33]. The higher order terms will come small and disposable under a slowly varying condition $\xi = x - ct$. Therefore, the soliton is given to the lowest order by the solutions of

$$u_t + 2ku_x - u_{xxt} + auu_x = 0. \tag{1.2}$$

According to Eq (1.2), Wazwaz proposed two modified forms of CH equation

$$u_t + 2ku_x - u_{xxt} + au^n u_x = 0, \tag{1.3}$$

and

$$u_t + 2ku_x - u_{xxt} + au^n (u^n)_x = 0, \tag{1.4}$$

where $a > 0, k \in R$, n is the strength of the nonlinearity [34, 35]. Under this sense, Wazwaz further presented two variants of (2+1)-dimensional Camassa-Holm-KP(CH-KP) equations

$$(u_t + 2ku_x - u_{xxt} - au^n u_x)_x + u_{yy} = 0, \tag{1.5}$$

and

$$(u_t + 2ku_x - u_{xxt} + au^n (u^n)_x)_x + u_{yy} = 0. \tag{1.6}$$

Since Eqs (1.5) and (1.6) are derived from the modified CH equations (1.3) and (1.4), which are similar to the deduction of the Kadomtsev-Petviashvili equation, thus they are called the "Camassa-Holm-KP equation" [36].

With the help of simulation method and dynamical system theory, Xie derived loops, periodic cusp waves, kinks, and peakons of a generalized (2+1)-dimensional CH-KP equation [37]. Biswas obtained analytic 1-soliton solution of two generalized CH-KP equations [38]. Tian investigated breathers, rogue waves and other kinds of solitary waves of a generalized CH-KP equation, through bilinear formalism and homoclinic breather limit approach [39]. Lai studied solitary patterns, periodic and algebraic traveling wave solutions for two generalized (2+1)-dimensional CH-KP equations by direct integration [40]. As for (3+1)-dimensional cases, a generalized (3+1)-dimensional time fractional CH-KP equation was educed in the sense of Riemann-Liouville fractional derivatives with the help of Agrawal's method, Euler-Lagrange equation and semi-inverse method [41].

On the other hand, by adding u_{tt} to the KP equation, Wazwaz introduced a generalized KP-Boussinesq equation

$$u_{xxxy} + 3(u_x u_y)_x + u_{tx} + u_{ty} + u_{tt} - u_{zz} = 0,$$

which makes a significant impact on the phase shift and the dispersion relation [42]. In this paper, following the same manners of Wazwaz, we propose an extension to the CH-KP equation:

$$(u_t + \alpha u_x + \beta u u_x + \gamma u_{xxt})_x + \lambda u_{tt} + \delta u_{yy} = 0, \tag{1.7}$$

where $u = u(x, y, t)$ is the height of the water's free surface over a flat bottom; $\alpha, \beta, \gamma, \lambda, \delta$ are nonzero constants. Equation (1.7) simulates the dispersion's role in the development of patterns in a liquid drop, and describes left and right traveling waves like the Boussinesq equation.

To our knowledge, the rational and generalized rational solution has not been reported for Eq (1.7) yet. Therefore, in this paper, we intend to find rational and generalized rational solutions of Eq (1.7) with the help of bilinear form and symbolic computation. In Section 2, we derive the second order, third order and fourth order rational solutions and explore the inner connections between the bilinear equation and rational solution by discussing the relevance between the complex roots and the formation of the waves. In Section 3, we obtain generalized rational solutions with two arbitrary parameters, that can be used to modulate the evolution progress. The detailed dynamical behaviors for the generalized rational solutions are discussed in Section 4, including the scatter behavior, exact locations where lump waves space, and the moving path. In Section 5, we analyze the multiple dark wave solitons. Section 6 contains the summary of this paper.

2. Rational solutions of Eq (1.7)

In this section, we will construct rational solutions of Eq (1.7) and assess the inner link between the bilinear equation and rational solution. Taking $\xi = x + t$, Eq (1.7) will be translated to

$$(\alpha + \lambda + 1)u_{\xi\xi} + \beta(u_\xi^2 + uu_{\xi\xi}) + \gamma u_{\xi\xi\xi\xi} + \delta u_{yy} = 0, \tag{2.1}$$

where $\alpha, \lambda, \beta, \gamma, \delta$ are real parameters. Using the transform $u = \frac{6\gamma}{\beta}(\ln f)_{\xi\xi}$, (2.1) becomes

$$\left(\delta D_y^2 + (\alpha + \lambda + 1)D_\xi^2 + \gamma D_\xi^4\right)F \cdot F = 0,$$

which is equal to

$$\delta(-2F_y^2 + 2FF_{yy}) + (\alpha + \lambda + 1)(-2F_\xi^2 + 2FF_{\xi\xi}) + \gamma(6F_{\xi\xi}^2 - 8F_\xi F_{\xi\xi\xi} + 2FF_{\xi\xi\xi\xi}) = 0. \tag{2.2}$$

As we can see, the bilinear equation (2.2) has three parts, and α, λ serve as the same effect in the second part. Therefore, in order to facilitate the following computation, we treat α, λ as the same parameter(setting $\alpha + \lambda = \alpha$). Of course, one can retrieves the original result by replacing α with $\alpha + \lambda$. With the help of bilinear form (2.2), the rational solution of Eq (1.7) can be obtained by the following theorem.

Theorem 2.1. *The generalized CH-KP equation (1.7) has rational solution*

$$u_n(\xi, y) = \frac{6\gamma}{\beta}\frac{\partial^2}{\partial\xi^2}\ln F_n(\xi, y), \tag{2.3}$$

with

$$F_n(\xi, y) = \sum_{j=0}^{n(n+1)/2}\sum_{i=0}^{j} a_{i,j}\xi^{2i}y^{2(j-i)}, \tag{2.4}$$

where $a_{i,j}$ is real parameter, $\beta, F_n \neq 0$ in order to make u_n analytic [43].

Using upon procedure one has

$$
\begin{aligned}
F_2(\xi,y) &= \xi^6 - \frac{25\gamma}{\alpha+1}\xi^4 - \frac{125\gamma(\alpha\gamma+\gamma)}{(\alpha+1)^3}\xi^2 + \frac{(\alpha+1)^3}{\delta^3}y^6 + \left(\frac{3\left(\alpha^2+2\alpha+1\right)}{\delta^2}\xi^2 - \frac{17(\alpha\gamma+\gamma)}{\delta^2}\right)y^4 \\
&+\left(\frac{3(\alpha+1)}{\delta}\xi^4 - \frac{90\gamma}{\delta}\xi^2 + \frac{475\gamma^2}{(\alpha+1)\delta}\right)y^2 - \frac{1875\gamma^3}{(\alpha+1)^3}, \\
F_3(\xi,y) &= \xi^{12} - \frac{98\gamma}{\alpha+1}\xi^{10} + \frac{735\gamma^2}{(\alpha+1)^2}\xi^8 - \frac{75460\gamma^3}{3(\alpha+1)^3}\xi^6 - \frac{5187875\gamma^4}{3(\alpha+1)^4}\xi^4 - \frac{159786550\gamma^5}{3(\alpha+1)^5}\xi^2 \\
&+\frac{(\alpha+1)^6}{\delta^6}y^{12} + \left(\frac{6(\alpha+1)^5}{\delta^5}\xi^2 - \frac{58(\alpha+1)^4\gamma}{\delta^5}\right)y^{10} + \left(\frac{15(\alpha+1)^4}{\delta^4}\xi^4 - \frac{570(\alpha+1)^3\gamma}{\delta^4}\xi^2\right. \\
&\left.+\frac{4335(\alpha+1)^2\gamma^2}{\delta^4}\right)y^8 + \left(\frac{20(\alpha+1)^3}{\delta^3}\xi^6 - \frac{1460(\alpha+1)^2\gamma}{\delta^3}\xi^4 + \frac{35420\left(\alpha\gamma^2+\gamma^2\right)}{\delta^3}\xi^2\right. \\
&\left.-\frac{798980\gamma^3}{3\delta^3}\right)y^6 + \left(\frac{15\left(\alpha^2+2\alpha+1\right)}{\delta^2}\xi^8 - \frac{1540(\alpha\gamma+\gamma)}{\delta^2}\xi^6 + \frac{37450\gamma^2}{\delta^2}\xi^4 + \frac{14700\gamma^3}{(\alpha+1)\delta^2}\xi^2\right. \\
&\left.+\frac{16391725\gamma^4}{3(\alpha+1)^2\delta^2}\right)y^4 + \left(\frac{6(\alpha+1)}{\delta}\xi^{10} - \frac{690\gamma}{\delta}\xi^8 + \frac{18620\gamma^2}{(\alpha+1)\delta}\xi^6 - \frac{220500\gamma^3}{(\alpha+1)^2\delta}\xi^4 + \frac{565950\gamma^4}{(\alpha+1)^3\delta}\xi^2\right. \\
&\left.-\frac{300896750\gamma^5}{3(\alpha+1)^4\delta}\right)y^2 + \frac{878826025\gamma^6}{9(\alpha+1)^6}, \\
F_4(\xi,y) &= \xi^{20} + 270\gamma\xi^{18} + 16605\gamma^2\xi^{16} + 351000\gamma^3\xi^{14} - 18877950\gamma^4\xi^{12} + 2094264900\gamma^5\xi^{10} \\
&-178095030750\gamma^6\xi^8 + 6967194507000\gamma^7\xi^6 + 190578711448125\gamma^8\xi^4 - 696163557521250\gamma^9\xi^2 \\
&+y^{20} + \left(10\xi^2+150\gamma\right)y^{18} + \left(45\xi^4+2190\gamma\xi^2+23085\gamma^2\right)y^{16} + \left(120\xi^6+11400\gamma\xi^4\right. \\
&\left.+354600\gamma^2\xi^2+3299400\gamma^3\right)y^{14} + \left(210\xi^8+31080\gamma\xi^6+1619100\gamma^2\xi^4+35645400\gamma^3\xi^2\right. \\
&\left.+360709650\gamma^4\right)y^{12} + \left(252\xi^{10}+50820\gamma\xi^8+3601080\gamma^2\xi^6+94613400\gamma^3\xi^4+671510700\gamma^4\xi^2\right. \\
&\left.+21813668100\gamma^5\right)y^{10} + \left(210\xi^{12}+52500\gamma\xi^{10}+4513950\gamma^2\xi^8+151237800\gamma^3\xi^6+2667498750\gamma^4\xi^4\right. \\
&\left.+31477666500\gamma^5\xi^2+1200881855250\gamma^6\right)y^8 + \left(120\xi^{14}+34440\gamma\xi^{12}+3308760\gamma^2\xi^{10}+135286200\gamma^3\xi^8\right. \\
&\left.+3824793000\gamma^4\xi^6+45237339000\gamma^5\xi^4+1982064357000\gamma^6\xi^2+43199536653000\gamma^7\right)y^6 \\
&+\left(45\xi^{16}+13800\gamma\xi^{14}+1367100\gamma^2\xi^{12}+56586600\gamma^3\xi^{10}+1071960750\gamma^4\xi^8+636363000\gamma^5\xi^6\right. \\
&\left.-405853402500\gamma^6\xi^4+90898176915000\gamma^7\xi^2+348683786758125\gamma^8\right)y^4 + \left(10\xi^{18}+3030\gamma\xi^{16}\right. \\
&\left.+275400\gamma^2\xi^{14}+10621800\gamma^3\xi^{12}+107534700\gamma^4\xi^{10}+4871002500\gamma^5\xi^8-521628471000\gamma^6\xi^6\right. \\
&\left.+33286514625000\gamma^7\xi^4+870343420196250\gamma^8\xi^2+3474517664913750\gamma^9\right)y^2+5917390238930625\gamma^{10}.
\end{aligned}
$$

Remark 2.1. *The solutions plotted in Figure 1 can be thought of as bound states of individual solitons, namely, two-, three- and four-humped multisolitons [44].*

We can derive two kinds of waves by choosing different coordinates. For instance, choosing (ξ, y), we can derive multi-lump soliton and (x, t) for multi-wave soliton. Firstly, let us consider the multi-lump soliton. The second order, third order and fourth order rational solutions are illustrated in Figure 1, showing two, three, four lumps under the conditions: $\alpha = \delta = -\gamma = 1, \beta = -6$ for Figure 1(a) and (b); $\alpha = -2, \delta = -1, \gamma = 1, \beta = 6$ for Figure 1(c). Second order rational solution u_2 has two separated peaks while there is one shaper peak in the middle surrounded by two shorter peaks for u_3. As for u_4, it has four divided peaks, two in the middle and two guarding around. Apparently, we can conclude that the nth order rational solution u_n has n separated peaks and the maximum value locates at $y = 0$ with n maximum values of u_n. On the other hand, multi-wave solitons are shown in Figures 2–4. According to the evolutional plots, these waves stem from a plain wave background and hit the maximum amplitude at $y = 0$. Then, they disappear with time. Interestingly, we find that higher order multi-wave solitons may contain lower ones. For example, the two-wave soliton does exist in the evolution progress of the three-wave soliton (see Figure 3(a)) and the three-wave soliton does exist in the evolution progress of the four-wave soliton (see Figure 4(a)).

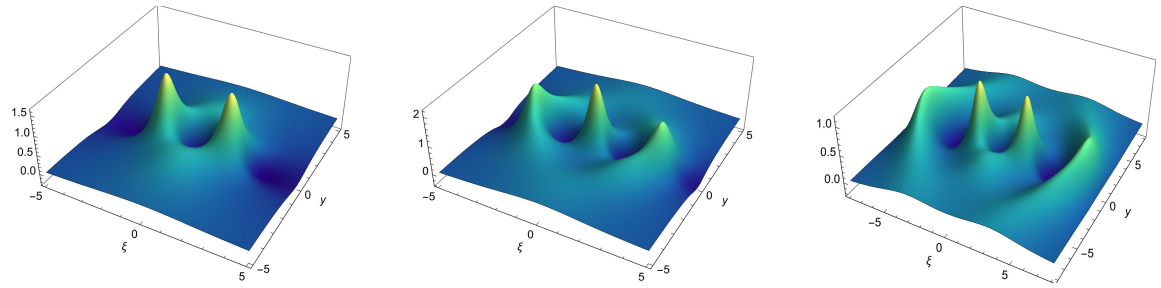

(a) (b) (c)

Figure 1. Rational solutions u_n in (ξ, y)-plane for $n = 2, 3, 4$ of Eq (1.7).

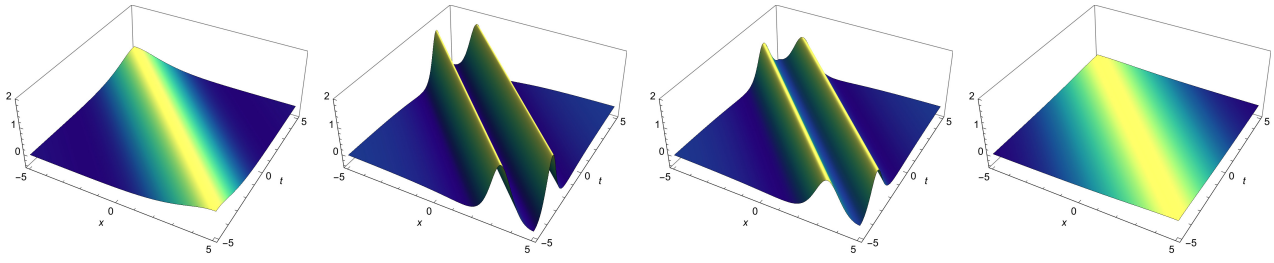

(a) y=−2 (b) y=0 (c) y=0.5 (d) y=5

Figure 2. Evolutional plots of the second order rational solution u_2 in (x, t)-plane with $\alpha = 1, \beta = -6, \gamma = -1, \sigma = 1$.

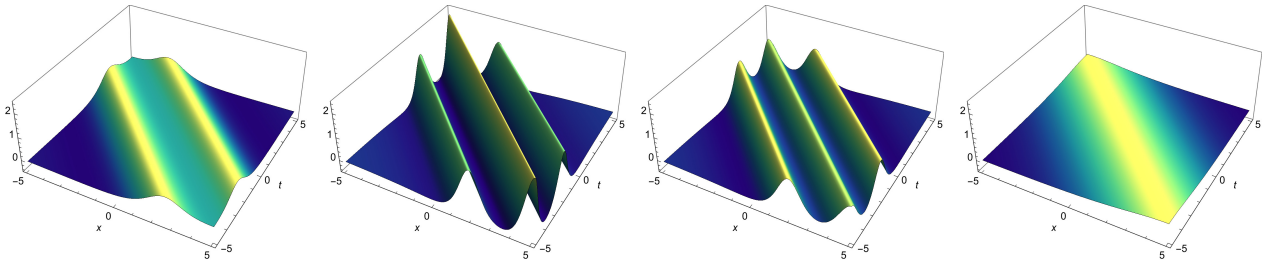

(a) y=−1.5 (b) y=0 (c) y=0.5 (d) y=4

Figure 3. Evolutional plots of the third order rational solution u_3 in (x,t)-plane with $\alpha = 1, \beta = -6, \gamma = -1, \sigma = 1$.

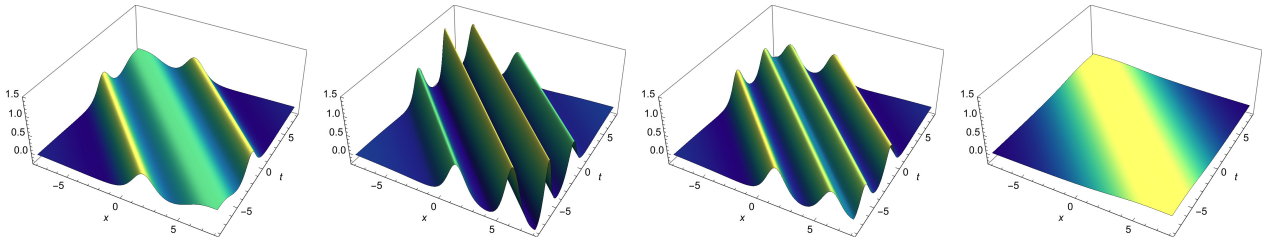

(a) y=−2 (b) y=0 (c) y=1 (d) y=10

Figure 4. Evolutional plots of the fourth order rational solution u_4 in (x,t)-plane with $\alpha = -2, \beta = 6, \gamma = 1, \sigma = -1$.

Remark 2.2. *Here, the solitons are plotted in (ξ,t)-plane and (x,t)-plane, and they are evolutionary of variable y. For some other models that transformed by $\xi = x + y$ in (2.1), the corresponding solutions will be evolutionary of t.*

In this part, we will look into the connection between polynomial F_n and rational solution u_n, through discussing the relevance between the complex roots and the formation of the waves. In Figure 5, each picture gives the complex root of $F_n = 0$ on the complex field, for $y = 0, y = 3n(n = 2, 3, 4)$ of x, i.e.,

$$\begin{cases} F_2(\xi,0) = 0 \\ F_2(\xi,6) = 0, \end{cases} \quad \begin{cases} F_3(\xi,0) = 0 \\ F_3(\xi,9) = 0, \end{cases} \quad \begin{cases} F_4(\xi,0) = 0 \\ F_4(\xi,12) = 0. \end{cases}$$

As shown in Figure 5, the red points are closer to the real axis than the blue points, which means the complex roots of $F_n = 0$ will leave the real axis when y grows. This result also accords with Figure 6. Above pictures demonstrate a "triangular pattern" for $y = 0, y = 3n$. For instance, the complex roots of $F_2(\xi,0) = 0$ construct two adjacent triangles, and the complex roots of $F_2(\xi,6) = 0$ form two divided triangles.

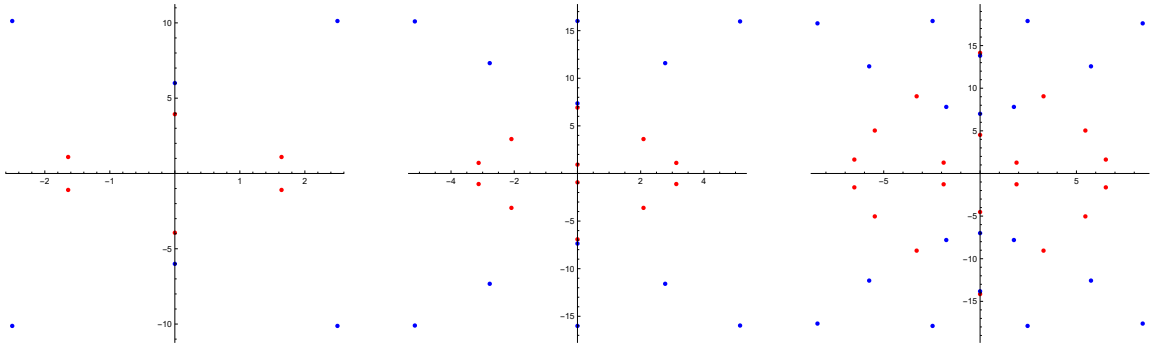

(a) $F_2(\xi, y)$ (b) $F_3(\xi, y)$ (c) $F_4(\xi, y)$

Figure 5. Complex roots of $F_n(\xi, y)$ for $n = 2, 3, 4$ with $y = 0$(red) and $y = 3n$(blue).

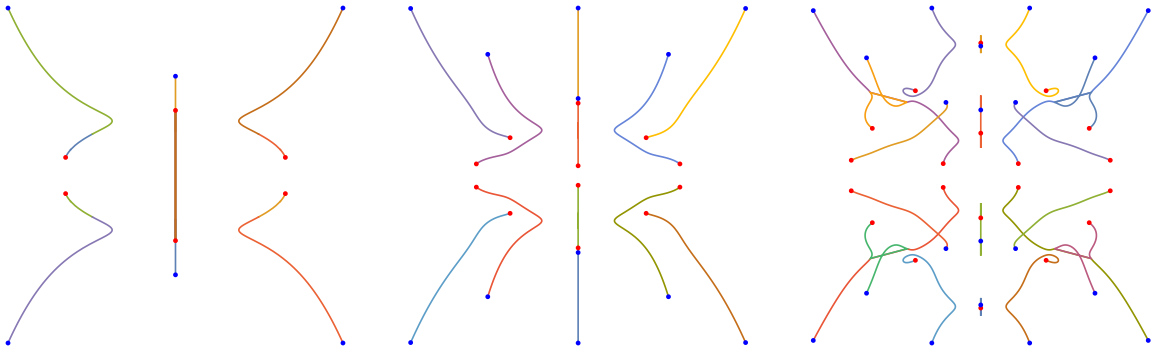

(a) $F_2(\xi, y)$ (b) $F_3(\xi, y)$ (c) $F_4(\xi, y)$

Figure 6. Loci of the complex roots of $F_n(\xi, y)$ for $n = 2, 3, 4$ as y varies.

We overlay the sectional view of u_4 on the map of the complex roots of $F_4(\xi, y) = 0$ in Figure 7. Unlike Figures 5 and 6, we choose six different values of y, that is $y = -15, -2, 0, 1, 4, 15$. As shown in Figure 7, the roots move to the real axis as y increases and $y = 0$ is the moment that those roots cluster together near the base point most closely. Next, they move away from the base point and form as isolated triangles like the initial condition. Together with the sectional view of u_4, we come to the conclusion that more complex roots around the base point, higher amplitude the wave has.

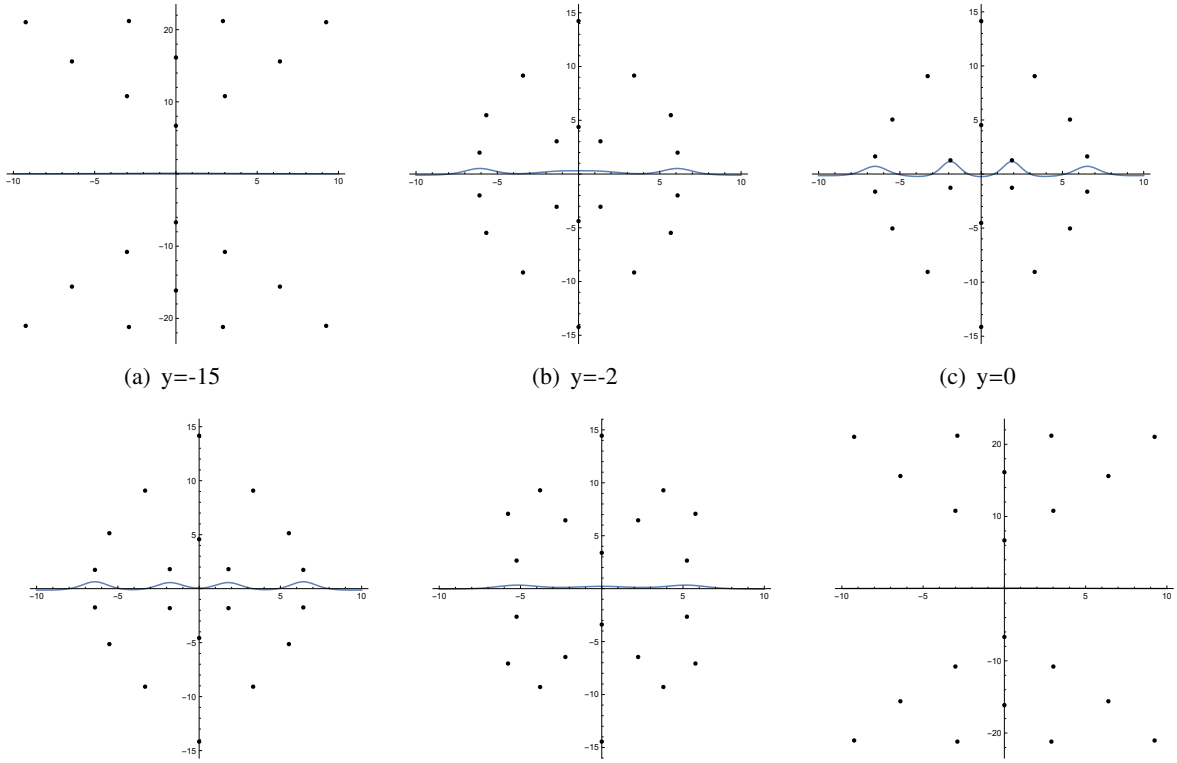

(a) y=-15 (b) y=-2 (c) y=0

(d) y=1 (e) y=4 (f) y=15

Figure 7. Plots of the loci of the complex roots of $F_4(\xi, y)$ and $u_4(\xi, y)$.

3. Generalized rational solutions of Eq (1.7)

Above, we have investigated the rational solutions of Eq (1.7) and assessed the inner link between the bilinear equation and the rational solution. Next, we are going to construct the generalized rational solutions of Eq (1.7) by introducing two free parameters μ, ν, which possess more complex mechanisms than their counterpart. In this case, the generalized rational solution also has two kinds of waves, multi-lump soliton and dark-multi-wave soliton (compare with the bright-multi-wave soliton in Section 2). With the help of bilinear form (2.2), the generalized rational solution of Eq (1.7) can be obtained by the following theorem.

Theorem 3.1. *The extended CH-KP equation (1.7) has generalized rational solution*

$$\bar{u}_n(\xi, y, \mu, \nu) = \frac{6\gamma}{\beta} \frac{\partial^2}{\partial \xi^2} \ln \bar{F}_n(\xi, y, \mu, \nu), \tag{3.1}$$

with

$$\bar{F}_{n+1}(\xi, y, \mu, \nu) = F_{n+1}(\xi, y) + 2\mu y P_n(\xi, y) + 2\nu\xi Q_n(\xi, y) + (\mu^2 + \nu^2) F_{n-1}(\xi, y), \tag{3.2}$$

and

$$P_n(\xi, y) = \sum_{j=0}^{n(n+1)/2} \sum_{i=0}^{j} b_{i,j} \xi^{2i} y^{2(j-i)}, \quad Q_n(\xi, y) = \sum_{j=0}^{n(n+1)/2} \sum_{i=0}^{j} c_{i,j} \xi^{2i} y^{2(j-i)},$$

where $\bar{F}_n \neq 0$ and $\mu, \nu, b_{i,j}, c_{i,j}$ are real parameters [43].

3.1. Second order generalized rational solution

Substituting $\bar{F}_2$ into (2.2) and equating the coefficients of all powers of ξ, y to zero, we have

$$
\begin{aligned}
&a_{0.0} = -\frac{1875\gamma^3 a_{3.3}}{(\alpha+1)^3} + \frac{\delta\mu^2 b_{1.1}^2 + 9(\alpha+1)\nu^2 c_{1.1}^2}{9(\alpha+1)a_{3.3}} - \mu^2 - \nu^2, \quad a_{0.1} = \frac{475\gamma^2 a_{3.3}}{(\alpha+1)\delta}, \quad a_{0.2} = -\frac{17(\alpha+1)\gamma a_{3.3}}{\delta^2},\\
&a_{0.3} = \frac{(\alpha+1)^3 a_{3.3}}{\delta^3}, \quad a_{1.1} = -\frac{125\gamma^2 a_{3.3}}{(\alpha+1)^2}, \quad a_{1.2} = -\frac{90\gamma a_{3.3}}{\delta}, \quad a_{1.3} = \frac{3(\alpha+1)^2 a_{3.3}}{\delta^2}, \quad a_{2.2} = -\frac{25\gamma a_{3.3}}{\alpha+1},\\
&a_{2.3} = \frac{3(\alpha+1)a_{3.3}}{\delta}, \quad b_{0.0} = -\frac{5\gamma b_{1.1}}{3(\alpha+1)}, \quad b_{0.1} = -\frac{(\alpha+1)b_{1.1}}{3\delta}, \quad c_{0.0} = \frac{\gamma c_{1.1}}{\alpha+1}, \quad c_{0.1} = -\frac{3(\alpha+1)c_{1.1}}{\delta},
\end{aligned}
\tag{3.3}
$$

where $a_{3.3}, b_{1.1}, c_{1.1}$ are arbitrary constants. Substituting into (3.1) and using $u = \frac{6\gamma}{\beta}(\ln f)_{\xi\xi}$, the solution of Eq (1.7) can be written as

$$
\bar{u}_2 = \frac{6\gamma}{\beta}(\ln \bar{F}_2(\xi, y, \mu, \nu))_{\xi\xi}.
$$

Here, $\alpha = -\gamma = \sigma = a_{3.3} = b_{1.1} = c_{1.1} = 1, \beta = -6$. Starting from the rational soliton $u_2(\xi, y)$ (see Figure 1(a)), the evolution plots of the generalized rational soliton $\bar{u}_2(\xi, y, \mu, \nu)$ are displayed in Figure 8. Numerical simulation indicates that there are two peaks for $\bar{u}_2(\xi, y, \mu, \nu)$ when μ, ν are small. One of the peaks shrinks, and divides into two small hills as μ, ν increase. After that, those tiny hills will rise up if μ, ν continue increase. Eventually $\bar{u}_2(\xi, y, \mu, \nu)$ contains three separated lump waves and organizes a triangle (see Figure 9).

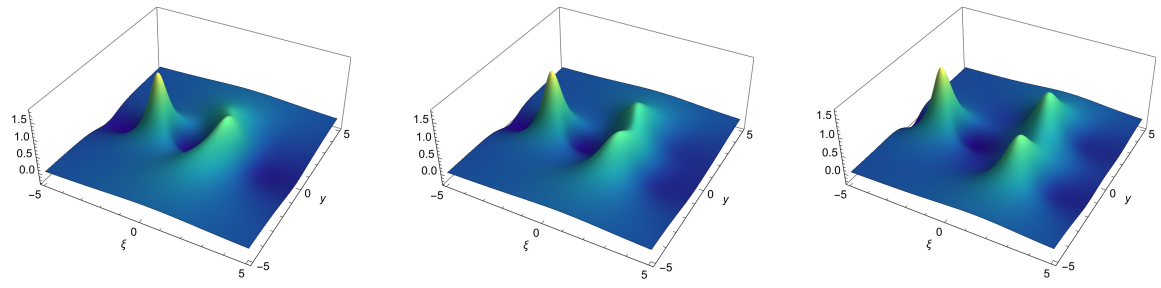

(a) $\mu = \nu = 10$ (b) $\mu = \nu = 20$ (c) $\mu = \nu = 40$

Figure 8. Evolutional plots of the generalized rational solution $\bar{u}_2$ in (ξ, y)-plane with $\alpha = 1, \beta = -6, \gamma = -1, \delta = 1, a_{3.3} = b_{1.1} = c_{1.1} = 1$ of Eq (1.7).

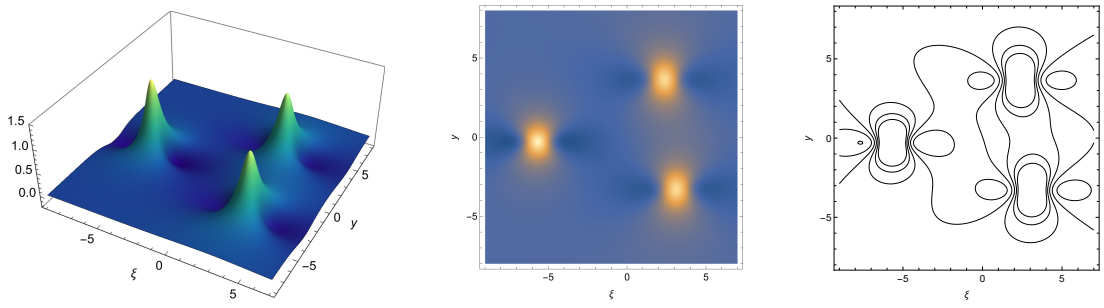

(a) Three-dimensional plot (b) Density plot (c) Contour plot

Figure 9. Generalized rational solution $\bar{u}_2$ in (ξ, y)-plane with $\alpha = 1, \beta = -6, \gamma = -1, \delta = 1, a_{3.3} = b_{1.1} = c_{1.1} = 1$ of Eq (1.7).

3.2. *Third order generalized rational solution*

Substituting $\bar{F}_3$ into (2.2) and equating the coefficients of all powers of ξ, y to zero, we have

$$a_{0.0} = \frac{878826025(\alpha+1)^2\gamma^6 - 27\gamma\left((\alpha+1)^7\nu^2 + \delta^7\mu^2\right)}{9(\alpha+1)^8\left(\mu^2+\nu^2+1\right)}, \quad a_{0.2} = \frac{16391725\gamma^4}{3(\alpha+1)^2\delta^2}, \quad a_{0.3} = -\frac{798980\gamma^3}{3\delta^3},$$

$$a_{0.1} = \frac{3\left((\alpha+1)^7\nu^2 + \delta^7\mu^2\right) - 300896750(\alpha+1)^2\gamma^5}{3(\alpha+1)^6\delta\left(\mu^2+\nu^2+1\right)}, \quad a_{0.4} = \frac{4335(\alpha+1)^2\gamma^2}{\delta^4}, \quad a_{0.5} = -\frac{58(\alpha+1)^4\gamma}{\delta^5},$$

$$a_{1.1} = \frac{3\left((\alpha+1)^7\nu^2 + \delta^7\mu^2\right) - 159786550(\alpha+1)^2\gamma^5}{3(\alpha+1)^7\left(\mu^2+\nu^2+1\right)}, \quad a_{0.6} = \frac{(\alpha+1)^6}{\delta^6}, \quad a_{1.2} = \frac{565950\gamma^4}{(\alpha+1)^3\delta},$$

$$a_{1.3} = \frac{14700\gamma^3}{(\alpha+1)\delta^2}, \quad a_{1.4} = \frac{35420\left(\alpha\gamma^2+\gamma^2\right)}{\delta^3}, \quad a_{1.5} = -\frac{570(\alpha+1)^3\gamma}{\delta^4}, \quad a_{1.6} = \frac{6(\alpha+1)^5}{\delta^5},$$

$$a_{2.2} = -\frac{5187875\gamma^4}{3(\alpha+1)^4}, \quad a_{2.3} = -\frac{220500\gamma^3}{(\alpha+1)^2\delta}, \quad a_{2.4} = \frac{37450\gamma^2}{\delta^2}, \quad a_{2.5} = -\frac{1460(\alpha+1)^2\gamma}{\delta^3},$$

$$a_{2.6} = \frac{15(\alpha+1)^4}{\delta^4}, \quad a_{3.3} = -\frac{75460\gamma^3}{3(\alpha+1)^3}, \quad a_{3.4} = \frac{18620\gamma^2}{(\alpha+1)\delta}, \quad a_{3.5} = -\frac{1540(\alpha\gamma+\gamma)}{\delta^2}, \quad a_{3.6} = \frac{20(\alpha+1)^3}{\delta^3},$$

$$a_{4.4} = \frac{735\gamma^2}{(\alpha+1)^2}, \quad a_{4.5} = -\frac{690\gamma}{\delta}, \quad a_{4.6} = \frac{15\left(\alpha^2+2\alpha+1\right)}{\delta^2}, \quad a_{5.5} = -\frac{98\gamma}{\alpha+1}, \quad a_{5.6} = \frac{6(\alpha+1)}{\delta},$$

$$b_{0.0} = -\frac{18865\gamma^3\delta^3}{3(\alpha+1)^6}, \quad b_{0.1} = -\frac{245\gamma^2\delta^2}{(\alpha+1)^4}, \quad b_{0.2} = \frac{7\gamma\delta}{(\alpha+1)^2}, \quad b_{1.1} = -\frac{665\gamma^2\delta^3}{(\alpha+1)^5}, \quad b_{1.2} = \frac{190\gamma\delta^2}{(\alpha+1)^3},$$

$$b_{1.3} = -\frac{9\delta}{\alpha+1}, \quad b_{2.2} = -\frac{105\gamma\delta^3}{(\alpha+1)^4}, \quad b_{2.3} = -\frac{5\delta^2}{(\alpha+1)^2}, \quad b_{3.3} = \frac{5\delta^3}{(\alpha+1)^3}, \quad c_{0.0} = -\frac{12005\gamma^3}{3(\alpha+1)^3},$$

$$c_{0.1} = \frac{535\gamma^2}{(\alpha+1)\delta}, \quad c_{0.2} = -\frac{45(\alpha\gamma+\gamma)}{\delta^2}, \quad c_{0.3} = \frac{5(\alpha+1)^3}{\delta^3}, \quad c_{1.1} = -\frac{245\gamma^2}{(\alpha+1)^2}, \quad c_{1.2} = \frac{230\gamma}{\delta},$$

$$c_{1.3} = -\frac{5\left(\alpha^2+2\alpha+1\right)}{\delta^2}, \quad c_{2.2} = -\frac{13\gamma}{\alpha+1}, \quad c_{2.3} = -\frac{9(\alpha+1)}{\delta}.$$

Substituting into (3.1) and using $u = \frac{6\gamma}{\beta}(\ln f)_{\xi\xi}$, the solution of Eq (1.7) can be written as

$$\bar{u}_3 = \frac{6\gamma}{\beta}(\ln \bar{F}_3(\xi, y, \mu, \nu))_{\xi\xi}.$$

Here, $\alpha = -\gamma = \sigma = 1, \beta = -6$. From Figure 1(b), we know that the rational solution $u_3(\xi, y)$ only has three peaks, with one in the middle and two guarding around. As μ, ν increases, two bilateral peaks start to split. To be specific, the left side peak divides into three, while the right side peak divides into two(see Figure 10). For sufficient large μ, ν, $\bar{u}_3(\xi, y, \mu, \nu)$ organizes a pentagon with one peak in the middle and five around it(see Figure 11).

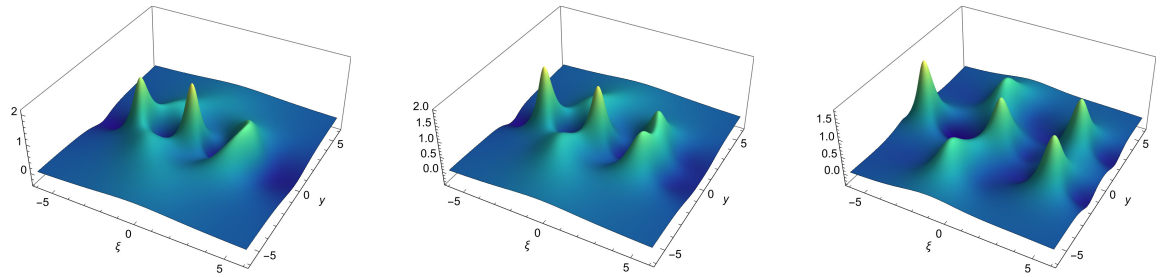

(a) $\mu = \nu = 400$ (b) $\mu = \nu = 1000$ (c) $\mu = \nu = 5000$

Figure 10. Evolutional plots of the generalized rational solution $\bar{u}_3$ in (ξ, y)-plane with $\alpha = 1, \beta = -6, \gamma = -1, \delta = 1$ of Eq (1.7).

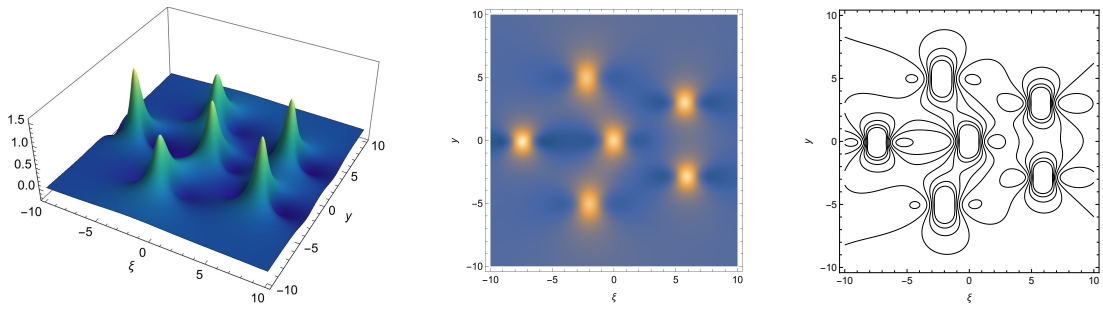

(a) Three-dimensional plot (b) Density plot (c) Contour plot

Figure 11. Generalized rational solution $\bar{u}_3$ in (ξ, y)-plane with $\alpha = 1, \beta = -6, \gamma = -1, \delta = 1$ of Eq (1.7).

3.3. Fourth order generalized rational solution

Substituting $\bar{F}_4$ into (2.2) and equating the coefficients of all powers of ξ, y to zero, we have

$$a_{9.9} = 270\gamma, \quad a_{9.10} = 10, \quad a_{8.8} = 16605\gamma^2, \quad a_{8.9} = 3030\gamma, \quad a_{8.10} = 45, \quad a_{7.7} = 351000\gamma^3,$$

$$a_{7.8} = 275400\gamma^2, \quad a_{7.9} = 13800\gamma, \quad a_{7.10} = 120, \quad a_{6.6} = -18877950\gamma^4, \quad a_{6.7} = 10621800\gamma^3,$$

$$a_{6.8} = 1367100\gamma^2, \quad a_{6.9} = 34440\gamma, \quad a_{6.10} = 210, \quad a_{5.5} = 2094264900\gamma^5, \quad a_{5.6} = 107534700\gamma^4,$$

$$a_{5.7} = 56586600\gamma^3, \quad a_{5.8} = 3308760\gamma^2, \quad a_{5.9} = 52500\gamma, \quad a_{5.10} = 252, \quad a_{4.4} = -178095030750\gamma^6,$$

$$a_{4.5} = 4871002500\gamma^5, \quad a_{4.6} = 1071960750\gamma^4, \quad a_{4.7} = 135286200\gamma^3, \quad a_{4.8} = 4513950\gamma^2,$$

$$a_{4.9} = 50820\gamma, \quad a_{4.10} = 210, \quad a_{3.3} = 6967194507000\gamma^7, \quad a_{3.4} = -521628471000\gamma^6,$$

$$a_{3.5} = 636363000\gamma^5, \quad a_{3.6} = 3824793000\gamma^4, \quad a_{3.7} = 151237800\gamma^3, \quad a_{3.8} = 3601080\gamma^2,$$

$$a_{3.9} = 31080\gamma, \quad a_{3.10} = 120, \quad a_{2.2} = 190578711448125\gamma^8, \quad a_{2.3} = 33286514625000\gamma^7,$$

$$a_{2.4} = -405853402500\gamma^6, \quad a_{2.5} = 45237339000\gamma^5, \quad a_{2.6} = 2667498750\gamma^4, \quad a_{2.7} = 94613400\gamma^3,$$

$$a_{2.8} = 1619100\gamma^2, \quad a_{2.9} = 11400\gamma, \quad a_{2.10} = 45, \quad a_{1.1} = -696163557521250\gamma^9,$$

$$a_{1.2} = 870343420196250\gamma^8, \quad a_{1.3} = 90898176915000\gamma^7, \quad a_{1.4} = 1982064357000\gamma^6,$$

$$a_{1.5} = 31477666500\gamma^5, \quad a_{1.6} = 671510700\gamma^4, \quad a_{1.7} = 35645400\gamma^3, \quad a_{1.8} = 354600\gamma^2,$$

$$a_{1.9} = 2190\gamma, \quad a_{1.10} = 10, \quad a_{0.0} = 5917390238930625\gamma^{10}, \quad a_{0.1} = 3474517664913750\gamma^9,$$

$$a_{0.2} = 348683786758125\gamma^8, \quad a_{0.3} = 43199536653000\gamma^7, \quad a_{0.4} = 1200881855250\gamma^6,$$

$$a_{0.5} = 21813668100\gamma^5, \quad a_{0.6} = 360709650\gamma^4, \quad a_{0.7} = 3299400\gamma^3, \quad a_{0.8} = 23085\gamma^2, \quad a_{0.9} = 150\gamma,$$

$$b_{0.6} = \frac{\sqrt{-c_{4.6}^2\nu^2 + 625\mu^2 + 625\nu^2}}{25\mu}, \quad b_{0.5} = \frac{2\gamma\sqrt{-c_{4.6}^2\nu^2 + 625\mu^2 + 625\nu^2}}{5\mu},$$

$$b_{1.6} = -\frac{18\sqrt{-c_{4.6}^2\nu^2 + 625\mu^2 + 625\nu^2}}{25\mu}, \quad b_{0.4} = -\frac{9\gamma^2\sqrt{-c_{4.6}^2\nu^2 + 625\mu^2 + 625\nu^2}}{\mu},$$

$$b_{1.5} = -\frac{262\gamma\sqrt{-c_{4.6}^2\nu^2 + 625\mu^2 + 625\nu^2}}{5\mu}, \quad b_{2.6} = -\frac{\sqrt{-c_{4.6}^2\nu^2 + 625\mu^2 + 625\nu^2}}{\mu},$$

$$b_{0.3} = \frac{684\gamma^3\sqrt{-c_{4.6}^2\nu^2 + 625\mu^2 + 625\nu^2}}{\mu}, \quad b_{1.4} = -\frac{15684\gamma^2\sqrt{-c_{4.6}^2\nu^2 + 625\mu^2 + 625\nu^2}}{5\mu},$$

$$b_{2.5} = -\frac{156\gamma\sqrt{-c_{4.6}^2\nu^2 + 625\mu^2 + 625\nu^2}}{5\mu}, \quad b_{3.6} = \frac{36\sqrt{-c_{4.6}^2\nu^2 + 625\mu^2 + 625\nu^2}}{25\mu},$$

$$b_{0.2} = \frac{443079\gamma^4\sqrt{-c_{4.6}^2\nu^2 + 625\mu^2 + 625\nu^2}}{\mu}, \quad b_{1.3} = -\frac{52668\gamma^3\sqrt{-c_{4.6}^2\nu^2 + 625\mu^2 + 625\nu^2}}{\mu},$$

$$b_{2.4}=\frac{4746\gamma^2\sqrt{-c_{4.6}^2\nu^2+625\mu^2+625\nu^2}}{\mu},\quad b_{3.5}=\frac{6132\gamma\sqrt{-c_{4.6}^2\nu^2+625\mu^2+625\nu^2}}{25\mu},$$

$$b_{4.6}=\frac{63\sqrt{-c_{4.6}^2\nu^2+625\mu^2+625\nu^2}}{25\mu},\quad b_{0.1}=\frac{6707610\gamma^5\sqrt{-c_{4.6}^2\nu^2+625\mu^2+625\nu^2}}{\mu},$$

$$b_{1.2}=-\frac{660618\gamma^4\sqrt{-c_{4.6}^2\nu^2+625\mu^2+625\nu^2}}{\mu},\quad b_{2.3}=\frac{33012\gamma^3\sqrt{-c_{4.6}^2\nu^2+625\mu^2+625\nu^2}}{\mu},$$

$$b_{5.6}=\frac{14\sqrt{-c_{4.6}^2\nu^2+625\mu^2+625\nu^2}}{25\mu},\quad b_{0.0}=-\frac{11764935\gamma^6\sqrt{-c_{4.6}^2\nu^2+625\mu^2+625\nu^2}}{\mu},$$

$$b_{1.1}=-\frac{11755926\gamma^5\sqrt{-c_{4.6}^2\nu^2+625\mu^2+625\nu^2}}{\mu},\quad b_{2.2}=\frac{384111\gamma^4\sqrt{-c_{4.6}^2\nu^2+625\mu^2+625\nu^2}}{\mu},$$

$$b_{3.3}=-\frac{5796\gamma^3\sqrt{-c_{4.6}^2\nu^2+625\mu^2+625\nu^2}}{\mu},\quad b_{4.4}=-\frac{105\gamma^2\sqrt{-c_{4.6}^2\nu^2+625\mu^2+625\nu^2}}{\mu},$$

$$b_{5.5}=-\frac{126\gamma\sqrt{-c_{4.6}^2\nu^2+625\mu^2+625\nu^2}}{5\mu},\quad b_{6.6}=-\frac{7\sqrt{-c_{4.6}^2\nu^2+625\mu^2+625\nu^2}}{25\mu},$$

$$c_{6.6}=-\frac{c_{4.6}}{25},\quad c_{5.5}=\frac{-74}{25}\gamma c_{4.6},\quad c_{5.6}=\frac{18c_{4.6}}{25},\quad c_{4.4}=33\gamma^2c_{4.6},\quad c_{4.5}=\frac{374}{5}\gamma c_{4.6},$$

$$c_{3.3}=-1692\gamma^3c_{4.6},\quad c_{3.4}=\frac{5316}{5}\gamma^2c_{4.6},\quad c_{3.5}=\frac{348}{5}\gamma c_{4.6},\quad c_{3.6}=-\frac{36c_{4.6}}{25},\quad c_{2.2}=89145\gamma^4c_{4.6},$$

$$c_{2.3}=13356\gamma^3c_{4.6},\quad c_{2.4}=294\gamma^2c_{4.6},\quad c_{2.5}=\frac{-1092}{5}\gamma c_{4.6},\quad c_{2.6}=-\frac{63c_{4.6}}{25},\quad c_{1.1}=-3130218\gamma^5c_{4.6},$$

$$c_{1.2}=-675990\gamma^4c_{4.6},\quad c_{1.3}=-52164\gamma^3c_{4.6},\quad c_{1.4}=-5964\gamma^2c_{4.6},\quad c_{1.5}=\frac{-378}{5}\gamma c_{4.6},$$

$$c_{1.6}=-\frac{14c_{4.6}}{25},\quad c_{0.0}=1799343\gamma^6c_{4.6},\quad c_{0.1}=15804054\gamma^5c_{4.6},\quad c_{0.2}=758961\gamma^4c_{4.6},$$

$$c_{0.3}=24948\gamma^3c_{4.6},\quad c_{0.4}=609\gamma^2c_{4.6},\quad c_{0.5}=\frac{294}{25}\gamma c_{4.6},\quad c_{0.6}=\frac{7c_{4.6}}{25}.$$

where $c_{4,6}$ is an arbitrary constant. Substituting into (3.1) and using $u=\frac{6\gamma}{\beta}(\ln f)_{\xi\xi}$, the solution of Eq (1.7) can be written as

$$\bar{u}_4=\frac{6\gamma}{\beta}(\ln\bar{F}_4(\xi,y,\mu,\nu))_{\xi\xi}.$$

Here, $\alpha=-2,\beta=6,\gamma=1,\sigma=-1$. The evolution of $\bar{u}_4(\xi,y,\mu,\nu)$ is a bit more complicated than the lower order ones. In Figure 12, two guarding peaks divide into four separated peaks, as another three tiny hills rise nearby the central peaks. For sufficient large μ,ν, $\bar{u}_4(\xi,y,\mu,\nu)$ possesses one double-peak wave in the middle and seven in a ring around it, composing a heptagram(see Figure 13).

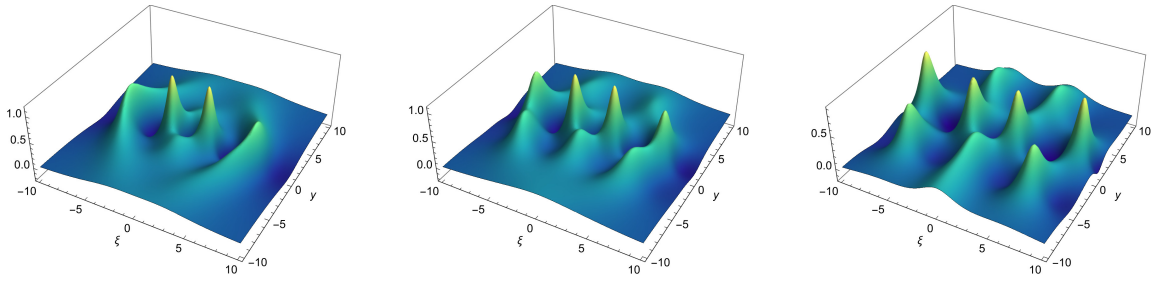

(a) $\mu = \nu = 1 \times 10^5$ (b) $\mu = \nu = 1 \times 10^6$ (c) $\mu = \nu = 5 \times 10^6$

Figure 12. Evolutional plots of the generalized rational solution $\bar{u}_4$ in (ξ, y)-plane with $\alpha = -2, \beta = 6, \gamma = 1, \delta = -1$ of Eq (1.7).

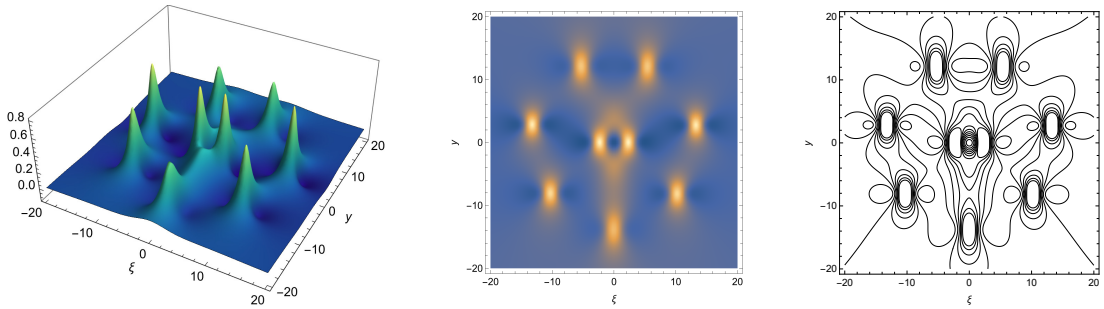

(a) Three-dimensional plot (b) Density plot (c) Contour plot

Figure 13. Generalized rational solution $\bar{u}_4$ in (ξ, y)-plane with $\alpha = -2, \beta = 6, \gamma = 1, \delta = -1$ of Eq (1.7).

Remark 3.1. *The multi-breather soliton that has similar structure such as forming a triangle, a pentagon and a heptagram can be seen in a generalized KP-BBM equation [45].*

4. Scatter of the lumps

Next, we will study the scatter behavior of the multi-lump soliton by selecting different μ, ν. Based on previous discussion, we know that $\bar{u}_n$ is capable of scattering to three-, six- and eight-lump waves as μ, ν increases. It is natural to wonder, what will happen if these parameters continue to increase? Therefore, we choose three different values of μ, ν for each solution to analyze their behavior. According to Figures 14–16, $\bar{u}_2, \bar{u}_3, \bar{u}_4$ own homologous character: if μ, ν continue to rise, the lumps will maintain their shape and expand the clearance to a larger picture.

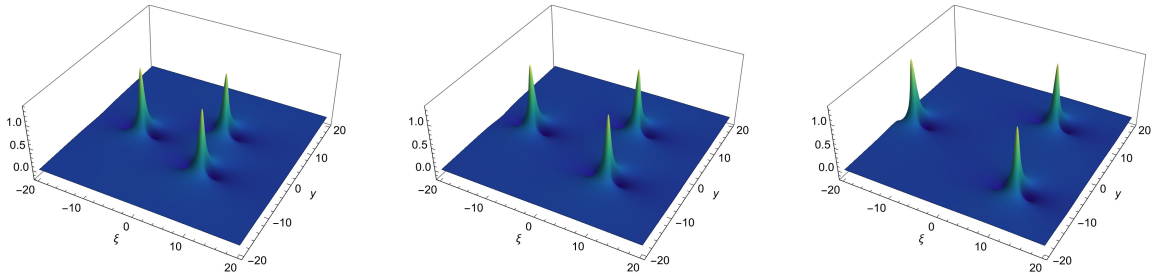

(a) $\mu = \nu = 1000$ (b) $\mu = \nu = 2000$ (c) $\mu = \nu = 5000$

Figure 14. Plots for the generalized rational solution $\bar{u}_2$ for various values of μ, ν.

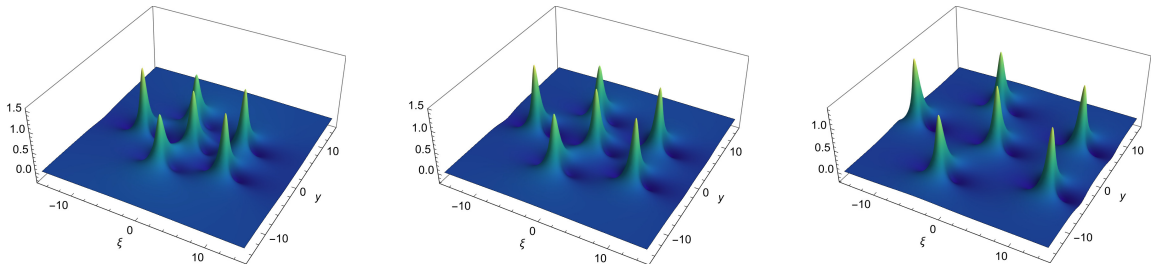

(a) $\mu = \nu = 4 \times 10^4$ (b) $\mu = \nu = 1 \times 10^5$ (c) $\mu = \nu = 4 \times 10^5$

Figure 15. Plots for the generalized rational solution $\bar{u}_3$ for various values of μ, ν.

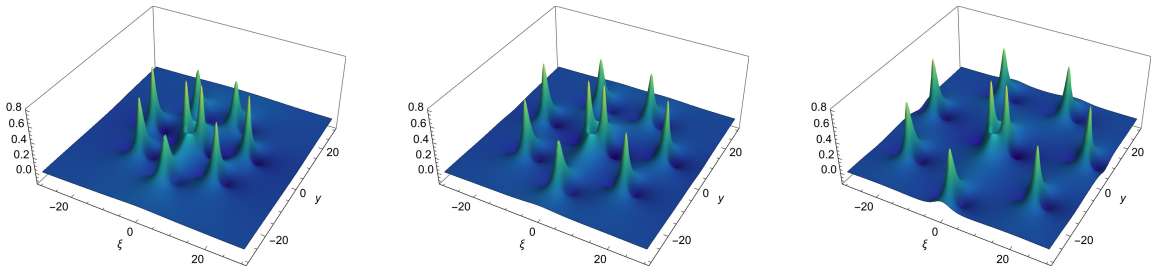

(a) $\mu = \nu = 2 \times 10^8$ (b) $\mu = \nu = 1 \times 10^9$ (c) $\mu = \nu = 5 \times 10^9$

Figure 16. Plots for the generalized rational solution $\bar{u}_4$ for various values of μ, ν.

According to above analysis, we know that if μ, ν continues to increase, these separated lumps will keep their formation and extend over a wider space. Obviously, the propagation observes a specific pattern. For this purpose, we will calculate the exact locations where extremum are and discuss their features. Under the same parametric conditions in Section 3, solve $\partial \bar{u}_n/\partial \xi = 0, \partial \bar{u}_n/\partial y = 0$ and omit extra point, we can obtain the location of extremum. Consequently, one has the following three circumcircles (see Figure 17)

$$(\xi - 0.029)^2 + (y + 0.038)^2 = 762.511,$$

$$(\xi + 0.030)^2 + (y - 0.122)^2 = 837.548,$$

$$(\xi - 0.052)^2 + (y + 0.191)^2 = 946.623,$$

where the lump waves locate, for $\bar{u}_2(\xi, y, 10^4, 10^4), \bar{u}_3(\xi, y, 10^7, 10^7), \bar{u}_4(\xi, y, 10^{10}, 10^{10})$, severally. It is noteworthy that during our calculation, the selection of the point is processed in a random order, and we find that other extremum accords with the same path.

We select several alternative values of μ, ν for each circumstance and overlay them in one picture. In Figure 18(a), we set $\mu = \nu = 6 \times 10^4, 2 \times 10^5, 5 \times 10^5, 1 \times 10^6$. In Figure 18(b), we set $\mu = \nu = 1 \times 10^7, 1 \times 10^8, 5 \times 10^8, 1.6 \times 10^9$. In Figure 18(c), we set $\mu = \nu = 5 \times 10^{10}, 4 \times 10^{11}, 2 \times 10^{12}, 7 \times 10^{12}$. Based on above superimposed contour plots, as μ, ν grows, the space between each other turns bigger, and the lump waves all move along a straight line in three, five, or seven different paths (red lines), respectively. Furthermore, except for $\bar{u}_2$, the higher order generalized rational solution has one stable solitary wave in the middle of the picture. Therefore, we have answered the query proposed at the beginning of Section 4: "what will happen if these parameters continue to increase?".

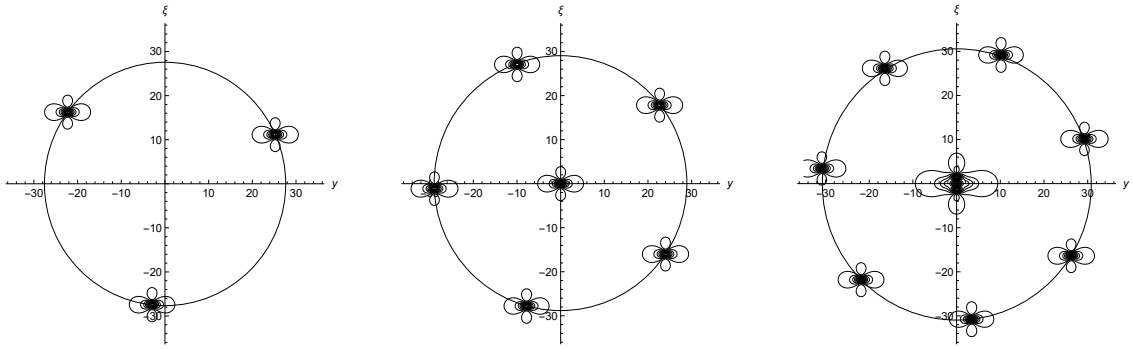

(a) $\bar{u}_2(\xi, y, 2 \times 10^4, 2 \times 10^4)$ (b) $\bar{u}_3(\xi, y, 2 \times 10^7, 2 \times 10^7)$ (c) $\bar{u}_4(\xi, y, 2 \times 10^{10}, 2 \times 10^{10})$

Figure 17. Contour plots of $\bar{u}_n$.

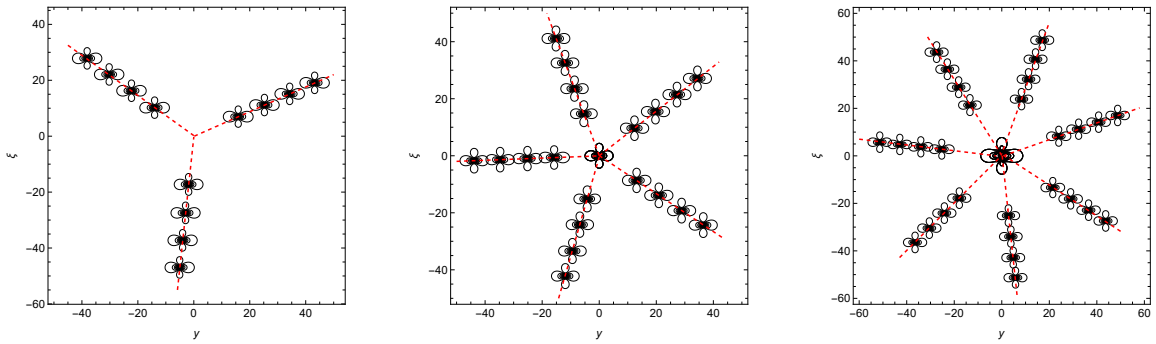

(a) $\bar{u}_2(\xi, y, \mu, \nu)$ (b) $\bar{u}_3(\xi, y, \mu, \nu)$ (c) $\bar{u}_3(\xi, y, \mu, \nu)$

Figure 18. Superimposed contour plots of $\bar{u}_n$.

5. Dark wave dynamics

For the generalized rational solution $\bar{u}_n$, it also has two appearances: multi-lump and multi-wave. Above, we have established the multi-lump soliton and studied its mechanism. Further, we will analyze the dark-multi-waves. Different from the bright-multi-waves obtained in Section 2, the dark-multi-waves do not come from a plain wave background and do not disappear with time. In Figure 19, there

is one stripe soliton hidden in the valley at the initial input $y = -0.2$. It starts to shrink at first, then rises up and forms two gullies. As for the second order generalized rational solution $\bar{u}_2$, there are three stripe solitons in the valley at the initial datum. Then, these stripe solitons converge into one and rise up above the surface (see Figure 20). The evolution of the third order generalized rational solution $\bar{u}_3$ is more complicated than the others. As is shown in Figure 21, there are three hidden stripe solitons in the middle at the beginning. Then, they converge into two and divide into three and finally leave us four gullies.

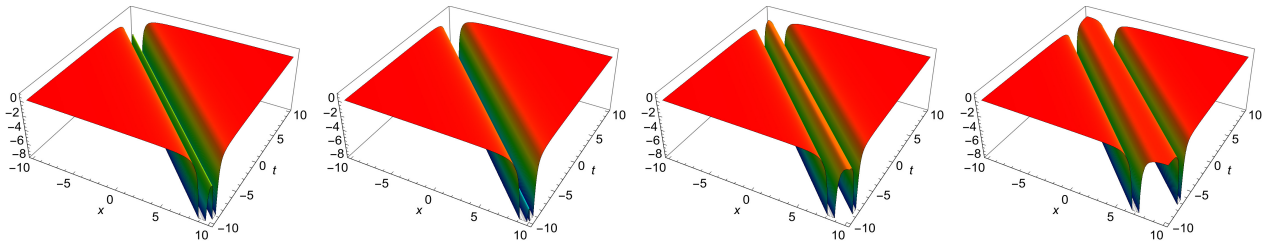

(a) y=-0.2 (b) y=0 (c) y=0.5 (d) y=1

Figure 19. Evolutional plots for the generalized rational solution $\bar{u}_1$ in (x, t)-plane with $\alpha = 10, \beta = -6, \gamma = -1, \sigma = -1$.

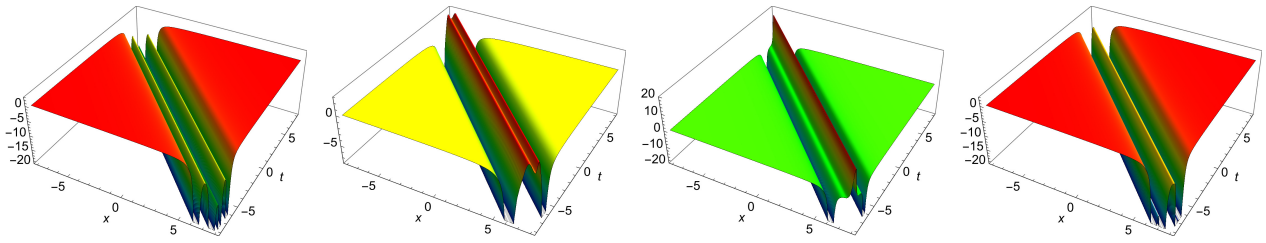

(a) y=-0.3 (b) y=0 (c) y=0.2 (d) y=0.4

Figure 20. Evolutional plots for the generalized rational solution $\bar{u}_2$ in (x, t)-plane with $\alpha = 10, \beta = -6, \gamma = -1, \sigma = -1, a_{3.3} = b_{1.1} = c_{1.1} = 1$.

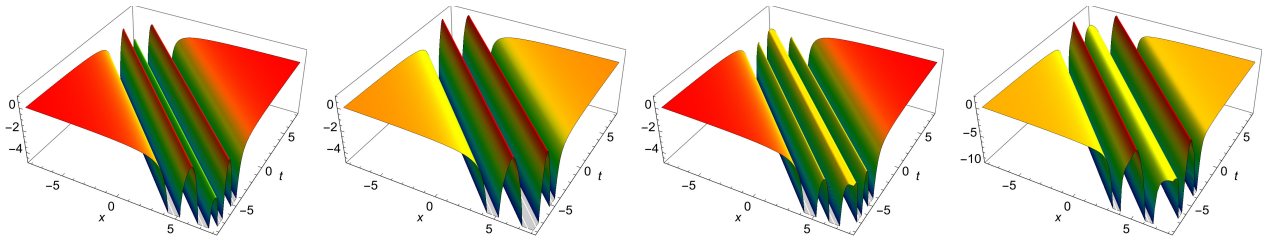

(a) y=-0.2 (b) y=0 (c) y=0.3 (d) y=1

Figure 21. Evolutional plots for the generalized rational solution $\bar{u}_3$ in (x, t)-plane with $\alpha = 10, \beta = -6, \gamma = -1, \sigma = -1$.

6. Conclusions

This paper proposes a new extension to the Camassa-Holm-Kadomtsev-Petviashvili (CH-KP) equation by adding an additional term u_{tt}, which simulates the dispersions role in the development of patterns in a liquid drop and describes left and right traveling waves like the Boussinesq equation. We have derived the rational and generalized rational solutions for this equation through its bilinear form and symbolic computation. By plotting them in different planes, two waveforms exist: multi-lump and multi-wave. Two-, three- and four-lump solitons are demonstrated in Figure 1. Except for the multi-lump soliton, we have plotted the multi-wave solitons in Figures 2–4, showing as multiple order line rogue waves. According to our numerical simulations, these waves stem from a plain wave background and hit the maximum amplitude at $y = 0$. Then, they disappear with time. Furthermore, we have explored the inner link between F_n and u_n by discussing the relevance between complex roots of $F_n = 0$ and the formation of waves. As for the generalized rational solution $\bar{u}_n$ with two free parameters μ, ν, we have systematically analyzed its scatter behavior by setting different μ, ν. The multiple order dark waves are introduced in Section 5, and they are different from the multi-wave solitons in Section 2. We believe these results may aid in explaining the progress of rogue waves, as they not only provide a complete picture of how a rogue wave can "come out of nowhere and disappear without a trace", but also makes it realistic in the actual world. Moreover, multi-component and higher order rational solutions demonstrating diverse interesting phenomena, particularly in fully discrete and (3+1)-dimensional cases, would be very interesting topics in future research.

Conflict of interest

The authors declare that they have no conflict of interest.

References

1. L. Draper, 'Freak' ocean waves, *Weather*, **21** (1966), 2–4. https://doi.org/10.1002/j.1477-8696.1966.tb05176.x
2. P. Muller, C. Garrett, A. Osborne, Rogue waves, *Oceanography*, **18** (2005), 66–75. http://dx.doi.org/10.5670/oceanog.2005.30
3. V. E. Zakharov, Stability of periodic waves of finite amplitude on the surface of a deep fluid, *J. Appl. Mech. Tech. Phys.*, **9** (1968), 190–194. https://doi.org/10.1007/BF00913182
4. A. Ankiewicz, N. Devine, N. Akhmediev, Are rogue waves robust against perturbations?, *Phys. Lett. A*, **373** (2009), 3997–4000. https://doi.org/10.1016/j.physleta.2009.08.053
5. N. Akhmediev, J. M. Soto-Crespo, A. Ankiewicz, Extreme waves that appear from nowhere: on the nature of rogue waves, *Phys. Lett. A*, **373** (2009), 2137–2145. https://doi.org/10.1016/j.physleta.2009.04.023
6. T. B. Benjamin, J. E. Feir, The disintegration of wave trains on deep water Part 1. Theory, *J. Fluid. Mech.*, **27** (1967), 417–430. https://doi.org/10.1017/S002211206700045X
7. A. M. Turing, The chemical basis of morphogenesis, *Bltn. Mathcal. Biology*, **52** (1990), 153–197. https://doi.org/10.1007/BF02459572

8. N. Akhmediev, A. Ankiewicz, J. M. Soto-Crespo, Rogue waves and rational solutions of the nonlinear Schrrödinger equation, *Phys. Rev. E*, **80** (2009), 026601. https://doi.org/10.1103/PhysRevE.80.026601

9. W. X. Ma, Lump solutions to the Kadomtsev-Petviashvili equation, *Phys. Lett. A*, **379** (2015), 1975–1978. https://doi.org/10.1016/j.physleta.2015.06.061

10. S. F. Tian, D. Guo, X. B. Wang, T. T. Zhang, Traveling wave, lump wave, rogue wave, multi-kink solitary wave and interaction solutions in a (3+1)-dimensional Kadomtsev-Petviashvili equation with Bäcklund transformation, *J. Appl. Anal. Comput.*, **11** (2021), 45–58. https://doi.org/10.11948/20190086

11. Z. Y. Yin, S. F. Tian, Nonlinear wave transitions and their mechanisms of (2+1)-dimensional Sawada-Kotera equation, *Physica D*, **427** (2021), 133002. https://doi.org/10.1016/j.physd.2021.133002

12. Z. Y. Wang, S. F. Tian, J. Cheng, The $\bar{\partial}$-dressing method and soliton solutions for the three-component coupled Hirota equations, *J. Math. Phys.*, **62** (2021), 093510. https://doi.org/10.1063/5.0046806

13. X. Wang, L. Wang, C. Liu, B. W. Guo, J. Wei, Rogue waves, semirational rogue waves and W-shaped solitons in the three-level coupled Maxwell-Bloch equations, *Commun. Nonlinear Sci.*, **107** (2022), 106172. https://doi.org/10.1016/j.cnsns.2021.106172

14. X. Wang, L. Wang, J. Wei, B. W. Guo, J. F. Kang, Rogue waves in the three-level defocusing coupled Maxwell-Bloch equations, *Proc. R. Soc. A*, **477** (2021), 20210585. https://doi.org/10.1098/rspa.2021.0585

15. J. C. Chen, Z. Y. Ma, Y. H. Hu, Nonlocal symmetry, Darboux transformation and soliton-cnoidal wave interaction solution for the shallow water wave equation, *J. Math. Anal. Appl.*, **460** (2018), 987–1003. https://doi.org/10.1016/j.jmaa.2017.12.028

16. X. Wang, J. Wei, Three types of Darboux transformation and general soliton solutions for the space-shifted nonlocal PT symmetric nonlinear Schrödinger equation, *Appl. Math. Lett.*, **130** (2022), 107998. https://doi.org/10.1016/j.aml.2022.107998

17. J. C. Chen, Z. Y. Ma, Consistent Riccati expansion solvability and soliton-cnoidal wave interaction solution of a (2+1)-dimensional Korteweg-de Vries equation, *Appl. Math. Lett.*, **64** (2017), 87–93. https://doi.org/10.1016/j.aml.2016.08.016

18. J. C. Chen, S. D. Zhu, Residual symmetries and soliton-cnoidal wave interaction solutions for the negative-order Korteweg-de Vries equation, *Appl. Math. Lett.*, **73** (2017), 136–142. https://doi.org/10.1016/j.aml.2017.05.002

19. X. Y. Gao, Y. J. Guo, W. R. Shan, Optical waves/modes in a multicomponent inhomogeneous optical fiber via a three-coupled variable-coefficient nonlinear Schrödinger system, *Appl. Math. Lett.*, **120** (2021), 107161. https://doi.org/10.1016/j.aml.2021.107161

20. X. Y. Gao, Y. J. Guo, W. R. Shan, Taking into consideration an extended coupled (2+1)-dimensional Burgers system in oceanography, acoustics and hydrodynamics, *Chaos Soliton. Fract.*, **161** (2022), 112293. https://doi.org/10.1016/j.chaos.2022.112293

21. X. Y. Gao, Y. J. Guo, W. R. Shan, Similarity reductions for a generalized (3+1)-dimensional variable-coefficient B-type Kadomtsev-Petviashvili equation in fluid dynamics, *Chinese J. Phys.*, **77** (2022), 2707–2712. https://doi.org/10.1016/j.cjph.2022.04.014

22. X. Y. Gao, Y. J. Guo, W. R. Shan, T. Y. Zhou, M. Wang, D. Y. Yang, In the atmosphere and oceanic fluids: scaling transformations, bilinear forms, Bäcklund transformations and solitons for a generalized variable-coefficient Korteweg-de Vries-modified Korteweg-de Vries equation, *China Ocean Eng.*, **35** (2021), 518–530. https://doi.org/10.1007/s13344-021-0047-7

23. X. Y. Gao, Y. J. Guo, W. R. Shan, D. Y. Yang, Bilinear forms through the binary Bell polynomials, N solitons and Bäcklund transformations of the Boussinesq-Burgers system for the shallow water waves in a lake or near an ocean beach, *Commun. Theor. Phys.*, **72** (2020), 095002. https://doi.org/10.1088/1572-9494/aba23d

24. X. Y. Gao, Y. J. Guo, W. R. Shan, D. Y. Yang, Regarding the shallow water in an ocean via a Whitham-Broer-Kaup-like system: hetero-Bäcklund transformations, bilinear forms and M solitons, *Chaos Soliton. Fract.*, **162** (2022), 112486. https://doi.org/10.1016/j.chaos.2022.112486

25. R. Camassa, D. D. Holm, An integrable shallow water equation with peaked solitons, *Phys. Rev. Lett.*, **71** (1993), 1661–1664. https://doi.org/10.1103/PhysRevLett.71.1661

26. Y. Zhang, H. Dong, X. Zhang, H. Yang, Rational solutions and lump solutions to the generalized (3+1)-dimensional shallow water-like equation, *Comput. Math. Appl.*, **73** (2017), 246–252. https://doi.org/10.1016/j.camwa.2016.11.009

27. T. B. Benjamin, J. L. Bona, J. J. Mahony, Model equations for long waves in nonlinear dispersive systems, *Phil. Trans. R. Soc. A*, **272** (1972), 47–78. https://doi.org/10.1098/rsta.1972.0032

28. A. Mekki, M. M. Ali, Numerical simulation of Kadomtsev-Petviashvili-Benjamin-Bona-Mahony equations using finite difference method, *Appl. Math. Comput.*, **219** (2013), 11214–11222. https://doi.org/10.1016/j.amc.2013.04.039

29. Y. Yin, B. Tian, X. Y. Wu, H. M. Yin, C. R. Zhang, Lump waves and breather waves for a (3+1)-dimensional generalized Kadomtsev-Petviashvili Benjamin-Bona-Mahony equation for an offshore structure, *Mod. Phys. Lett. B*, **32** (2018), 1850031. https://doi.org/10.1142/S0217984918500318

30. D. J. Korteweg, G. de Vries, On the change of form of long waves advancing in a rectangular canal, and on a new type of long stationary waves, *The London, Edinburgh, and Dublin Philosophical Magazine and Journal of Science*, **39** (1895), 422–443. https://doi.org/10.1080/14786449508620739

31. Z. Liu, R. Wang, Z. Jing, Peaked wave solutions of Camassa-Holm equation, *Chaos Soliton. Fract.*, **19** (2004), 77–92. https://doi.org/10.1016/S0960-0779(03)00082-1

32. W. Liu, Y. Zhang, Families of exact solutions of the generalized (3+1)-dimensional nonlinear-wave equation, *Mod. Phys. Lett. B*, **32** (2018), 1850359. https://doi.org/10.1142/S0217984918503591

33. J. P. Boyd, Peakons and cashoidal waves: travelling wave solutions of the Camassa-Holm equation, *Appl. Math. Comput.*, **81** (1997), 173–187. https://doi.org/10.1016/0096-3003(95)00326-6

34. A. M. Wazwaz, A class of nonlinear fourth order variant of a generalized Camassa-Holm equation with compact and noncompact solutions, *Appl. Math. Comput.*, **165** (2005), 485–501. https://doi.org/10.1016/j.amc.2004.04.029

35. A. M. Wazwaz, The Camassa-Holm-KP equations with compact and noncompact travelling wave solutions, *Appl. Math. Comput.*, **170** (2005), 347–360. https://doi.org/10.1016/j.amc.2004.12.002

36. A. M. Wazwaz, Exact solutions of compact and noncompact structures for the KP-BBM equation, *Appl. Math. Comput.*, **169** (2005), 700–712. https://doi.org/10.1016/j.amc.2004.09.061

37. S. L. Xie, L. Wang, Y. Z. Zhang, Explicit and implicit solutions of a generalized Camassa-Holm Kadomtsev-Petviashvili equation, *Commun. Nonlinear Sci.*, **17** (2012), 1130–1141. https://doi.org/10.1016/j.cnsns.2011.07.003

38. A. Biswas, 1-Soliton solution of the generalized Camassa-Holm Kadomtsev-Petviashvili equation, *Commun. Nonlinear. Sci.*, **14** (2009), 2524–2527. https://doi.org/10.1016/j.cnsns.2008.09.023

39. C. Y. Qin, S. F. Tian, X. B. Wang, T. T. Zhang, On breather waves, rogue waves and solitary waves to a generalized (2+1)-dimensional Camassa-Holm-Kadomtsev-Petviashvili equation, *Commun. Nonlinear Sci.*, **62** (2018), 378–385. https://doi.org/10.1016/j.cnsns.2018.02.040

40. S. Y. Lai, Y. Xu, The compact and noncompact structures for two types of generalized Camassa-Holm-KP equations, *Commun. Nonlinear Sci.*, **47** (2008), 1089–1098. https://doi.org/10.1016/j.mcm.2007.06.020

41. C. N. Lu, L. Y. Xie, H. W. Yang, Analysis of Lie symmetries with conservation laws and solutions for the generalized (3+1)-dimensional time fractional Camassa-Holm-Kadomtsev-Petviashvili equation, *Comput. Math. Appl.*, **77** (2019), 3154–3171. https://doi.org/10.1016/j.camwa.2019.01.022

42. A. M. Wazwaz, Solving the (3+1)-dimensional KP-Boussinesq and BKP-Boussinesq equations by the simplified Hirota's method, *Nonlinear Dyn.*, **88** (2017), 3017–3021. https://doi.org/10.1007/s11071-017-3429-x

43. P. A. Clarkson, E. Dowie, Rational solutions of the Boussinesq equation and applications to rogue waves, *Transactions of Mathematics and Its Applications*, **1** (2017), tnx003. https://doi.org/10.1093/imatrm/tnx003

44. D. E. Pelinovskii, Y. A. Stepanyants, New multisoliton solutions of the Kadomtsev–Petviashvili equation, *JETP Lett.*, **57** (1993), 24–28.

45. Y. Y. Xie, L. F. Li, Multiple-order breathers for a generalized (3+1)-dimensional Kadomtsev-Petviashvili Benjamin-Bona-Mahony equation near the offshore structure, *Math. Comput. Simulat.*, **193** (2021), 19–31. https://doi.org/10.1016/j.matcom.2021.08.021

AIMS Press